Pramana – J. Phys. (2021) 95:167
https://doi.org/10.1007/s12043-021-02202-0

A study of electron scattering from O_3 and its isovalent molecules from 0.1 to 5 keV

ANAND BHARADVAJA[1],*, SAVINDER KAUR[2] and KASTURI LAL BALUJA[3]

[1]Department of Physics, Bhaskaracharya College of Applied Sciences (University of Delhi), New Delhi 110 075, India
[2]Department of Physics, SGTB Khalsa College, University of Delhi, Delhi 110 007, India
[3]Formerly at: Department of Physics and Astrophysics, University of Delhi, Delhi 110 007, India
*Corresponding author. E-mail: anand_bharadvaja@yahoo.com

MS received 13 October 2020; revised 1 June 2021; accepted 2 June 2021
Abstract. The electron scatterings from isovalent molecules like O_3, S_3, OSO and SOS are studied using single centre expansion (SCE) approximation. The elastic differential cross-sections, integral and momentum transfer cross-sections are computed for these targets from ionisation threshold to 5 keV. The molecular wave functions of the targets were obtained from the multicentre expansion of the Gaussian-type orbitals within the single determinant Hartree–Fock self-consistent field scheme. The multipole expansion of the target at the centre of mass includes the dipole and quadrupole terms. The target interactions are modelled within the local potential approximation and consist of static, correlation-polarisation and exchange effects. The results are in good agreement with the available experimental and theoretical results. The SCE results match smoothly near the ionisation threshold with the *ab-initio* *R*-matrix results. This helped in estimating the scattering cross-section data from 0.1 to 5 keV energy. The total cross-sections obtained by summing the elastic and inelastic cross-sections are also in excellent agreement with the available results. The scattering study from isovalent molecules further helped in understanding the effects of dipole moment, polarisation and geometrical size while evaluating the collision problem.

Keywords. Electron scattering; single centre expansion; *R*-matrix; cross-sections; Hartree–Fock.

PACS Nos **34.80.Bm; 34.80.Gs; 34.80.Ht**

1. Introduction

In an isovalent molecular system, one of the atom of a molecule is replaced by its next row element. Molecules like SiN, CP, SiP form an isovalent set for the CN system. The targets chosen in the study are also isovalent molecules where one or more atoms of ozone is replaced by S atom(s). The isovalent molecules may have different ground states even if they belong to the same point group, e.g. CH_2 is a triplet but SiH_2 is a singlet. These types of molecules may also belong to different point groups and have different ground states C_2, CSi and Si_2. CSi is a polar molecule whose ground-state electronic configuration belongs to $C_{\infty v}$ point group whereas the other two molecules are non-polar and belong to $D_{\infty h}$ point group [1]. This implies that for a given set of isovalent system, the individual molecules may differ in reaction properties, electronic spectra and molecular properties like dipole moment and polarisability. This is bound to influence the electron–molecule scattering dynamics and may lead to surprising trends in scattering results well beyond our intuitive knowledge. In the absence of any definitive trends in molecular properties, the system of isovalent molecules therefore present an ideal case to investigate the trends in the electron impact scattering cross-sections. The O_3-based isovalent molecules considered, belonging to C_{2v} point group, have $^1A_1$ ground-state electronic symmetry but different cores. These molecules have relevance in astrophysics, atmospheric physics and technological plasma [2–8]. The electron–molecule interactions play important roles in understanding and modelling various electron-driven processes in many fields [9–11]. This essentially means that a comprehensive set of accurate electron–molecule collision cross-section data is required over a wide range of energy values.

These molecules have been extensively studied in low-energy range separately using *ab-initio* methods like *R*-matrix [12–16] and Schwinger multichannel approach [17–19]. A common feature in these studies

Published online: 09 October 2021

has been that these *ab-initio* methods did not include ionisation channel. The *R*-matrix approach could yield electronic excitation cross-sections in addition to elastic cross-sections [20,21]. The complications arising in computations due to the availability of a large number of channels could have been the reason for the neglect of ionisation channel. The *R*-matrix with pseudostates (RMPS) method has proved successful in yielding cross-sections only for small molecules up to 50 eV [22–25]. A more appealing simpler approach can be the use of local potentials to obtain cross-sections beyond ionisation. This approach has been widely used in conjunction with the additivity rule to obtain molecular collision cross-sections from the atomic constituents [26–29]. Several researchers have obtained molecular cross-sections using single centre expansion (SCE) formalism, but considering only the spherical molecular charge densities and local potentials [30–33]. This approach leads to the overestimation of cross-section data from 15 to 100 eV energy range due to the omission of anisotropic effects [34].

In the present study, we have invoked the SCE formalism [35–37] within the molecular framework to obtain various elastic scattering cross-sections such as elastic differential (DCS), integral elastic (ECS) and momentum transfer (MTCS) from ionisation threshold up to 5 keV. We have taken into consideration the anisotropy of molecules by considering higher-order partial waves in the bound-state expansion of molecular properties like wave function, potential and density of the molecules. The SCE approach is simplified by restricting it to the use of local potentials. The open channels contributing to scattering phenomenon are considered explicitly. The ionisation cross-sections are approximated by binary encounter Bethe (BEB) model [38].

Another aspect of this study has been the evaluation of SCE and *ab-initio* *R*-matrix results near the ionisation threshold. A smooth transition from *R*-matrix to SCE results has helped in estimating the collision data over extensive range of energies from 0.1 to 5 keV. It is underlined that these molecules were studied in the past in the low-energy region using the older versions of *R*-matrix based UKRmol codes [12–15]. The UKRmol codes have been updated several times since their first release [39,40]. The present calculations were redone using the UKRmol+ (version-1.0) [41] only for evaluating the trends in cross-sections upto the ionisation threshold. Hence, details like methodology, target modelling, convergence studies, resonances etc. are not emphasised. The interested readers can refer to the earlier papers for detailed understanding of the approach. The study has further helped to understand the effect of dipole moment and polarisation on electron scattering from isovalent molecules.

2. Methods and details

2.1 *Single centre expansion method*

The theory and details of single centre expansion method are outlined in a paper by Sanna and Gianturco [42]. We therefore, restrict ourselves to the relevant aspects only. In SCE formalism, the bound-state wave function for each electron of the target is expanded around the centre of mass (c.o.m.) of the N-electron molecular target as

$$u_i(\mathbf{r}) = \frac{1}{r}\sum_{l,h} u_{i,hl}(r) X_{hl}^{i,p\mu}(\theta,\phi), \tag{1}$$

where p refers to the irreducible representation (IR) for a particular type of point group in the ground state, h denotes a specific basis for a given partial wave l for μ, i is the specific multicentre orbital contributing to the density of bound electrons and $u_{i,hl}$ is the radial coefficient. $X_{lh}^{p\mu}(\theta,\phi)$ are the symmetry-adapted angular functions satisfying orthonormality conditions and are expressed as a linear combination of spherical harmonics $S_{lm}(\theta,\phi)$ and have the expansion coefficients all singly valued to one. The X's are then represented as

$$X_{lm}^{i,p\mu}(\theta,\phi) = \sum_{m=-l}^{+l} b_{lhm}^{p\mu} S_{lm}(\theta,\phi). \tag{2}$$

The coefficients b_{lhm} corresponding to a particular IR are given by the character table in [43]. For closed shell molecules $p\mu = A_1$.

The electron–molecule interactions for each target in the static exchange polarisation (SEP) approximation is described by static, correlation-polarisation and exchange potentials. The static potential is given by the sum of attractive interaction between the scattering electron and target containing N nuclei as well as the mean-field repulsion with the bound electrons.

$$V_{\mathrm{st}}(\mathbf{r}) = -\int \rho(\mathbf{s})\frac{1}{|\mathbf{r}-\mathbf{s}|}\mathrm{d}s + \sum_i^N \frac{Z_i}{|\mathbf{r}-\mathbf{R}_i|} \tag{3}$$

where R_i is the space coordinates of the nuclei.

The dynamical response of the target to the impinging electron is represented by correlation-polarisation potential (V_{cp}). The long- and short-range regions of V_{cp} are matched at some distance r_0 for the correct description of correlation polarisation.

$$V_{\mathrm{cp}}(\mathbf{r}) = \begin{cases} V_{\mathrm{corr}}(\mathbf{r}) & \text{for} \quad r \le r_0 \\ V_{\mathrm{pol}}(\mathbf{r}) & \text{for} \quad r > r_0. \end{cases} \tag{4}$$

V_{corr} given by Perdew and Zunger [44] is used in present calculations:

$$V_{\rm corr}(\mathbf{r}) = \begin{cases} (0.0311 + 0.00133 r_s)\ln r_s - 0.0084 r_s - 0.0584 & \text{for } r_s < 1.0, \\ \dfrac{\gamma(1 + \frac{7}{6}\beta_1 r_s^{1/2} + \frac{4}{3}\beta_2 r_s)}{(1 + \beta_1 r_s^{1/2} + \beta_2 r_s)^2} & \text{for } r_s \geq 1.0, \end{cases} \tag{5}$$

where $\gamma = -0.1423$, $\beta_1 = 1.0529$ and $\beta_2 = 0.3334$. $V_{\rm pol}$ is of the form

$$V_{\rm pol}(\mathbf{r}) = -\frac{1}{2r^6}\sum_{i,j} x_i x_j \alpha_{ij}, \tag{6}$$

where $r^2 = x_1^2 + x_2^2 + x_3^2$ and α_{ij} is the polarisability tensor.

The exchange potential is approximated by Hara [45] type energy-dependent free electron gas exchange (FEGE) model

$$V_{\rm ex}(\mathbf{r}) = -\frac{2}{\pi}K_F(\mathbf{r})\left[\frac{1}{2} + \frac{1-\eta^2}{4\eta}\ln\left|\frac{1+\eta}{1-\eta}\right|\right], \tag{7}$$

where $K_F(\mathbf{r}) = [3\pi^2\rho(\mathbf{r})]^{1/3}$ and $\eta = k/K_F$. The local momentum k is given by

$$k(\mathbf{r}) = [2(E_{\rm c} + I_{\rm P}) + K_F^2(\mathbf{r})]^{1/2}. \tag{8}$$

Here, $I_{\rm P}$ is the ionisation potential for the neutral target molecule and $E_{\rm c}$ is the collision energy. The total local interacting potential is the sum of three potentials:

$$V(\mathbf{r}) = V_{\rm st}(\mathbf{r}) + V_{\rm cp}(\mathbf{r}) + V_{\rm ex}(\mathbf{r}). \tag{9}$$

Once the potential is determined, the radial coefficients for $(N+1)$th continuum electron are obtained by solving the Schrödinger equation (in a.u.):

$$\left[\frac{{\rm d}^2}{{\rm d}r^2} - \frac{l(l+1)}{r^2} + k^2\right]\psi_{lh}^{p\mu}(r) = 2\sum_{l'h'} V_{lh,l'h'}^{A_1}(r)\psi_{l'h'}^{p\mu}(r), \tag{10}$$

where $k^2/2$ is the collision energy and $V_{lh,l'h'}(r)$ is the local potential coupling element which is given by

$$V_{lh,l'h'}^{A_1}(r) = \int {\rm d}\hat{r}\, X_{lh}^{p\mu}(\hat{r}) V(\mathbf{r}) X_{l'h'}^{p\mu}(\hat{r}). \tag{11}$$

Solving the equation under proper boundary conditions leads to the corresponding T-matrix elements from where the elastic cross-sections are obtained in body frame (BF) [46]:

$$\sigma_e^{\rm BF} = \frac{\pi}{k^2}\sum_{lh}\sum_{l'h'}|T_{lh,h'l'}|^2. \tag{12}$$

The DCS offers a more stringent test of any theory. These are required to obtain collision moments like momentum transfer cross-section (MTCS or Q_m) and viscosity cross-section [47], collision frequency, molecular Bremsstrahlung process etc. [13,48] and plasma parameters like transverse diffusion coefficient, modelling of transport phenomena in plasmas and gases [49]. The DCS for a polyatomic molecule can be expressed as

$$\frac{{\rm d}\sigma}{{\rm d}\Omega}(J\tau \to J'\tau') = \sum_L A_{\rm L} P_{\rm L}(\cos\theta), \tag{13}$$

where $P_{\rm L}(\cos\theta)$ is the Legendre polynomial and θ is the scattering angle. The scattering coefficient $A_{\rm L}$ is independent of scattering angle and is a function of incident energy [36]. The long-range nature of the dipolar potential results in poor convergence of the partial-wave expansion of DCS for electron scattering by polar molecules. Such limitations can be overcome by using Born approximation. The main idea is in adding and subtracting the Born dipole cross-sections to the partial wave expansion obtained from non- perturbative calculations. Since the Born approximation works very well for higher partial waves, this procedure speeds up convergence of the partial wave expansion very efficiently. The elastic DCS following Born top-up procedure [49] are given by

$$\frac{{\rm d}\sigma}{{\rm d}\Omega}(J\tau \to J'\tau') = \sum_{J'\tau'}\frac{{\rm d}\sigma^B}{{\rm d}\Omega} + \sum_L (A_{\rm L} - A_{\rm L}^{\rm B})P_{\rm L}(\cos\theta), \tag{14}$$

where $J\tau$ and $J'\tau'$ denote the initial and final rotational levels. The summation over L converges rapidly, as the electron–dipole interaction dominates the contribution from the higher partial waves. This electron–dipole interaction term is calculated in the first Born approximation for a rotating dipole. The coefficients $A_{\rm L}$ are computed from the K-matrices, which are in turn obtained by solving the close-coupling equations. The coefficients $A_{\rm L}^{\rm B}$ are computed from the K-matrices using the first Born approximation [36]. The final differential cross-section is thus the summation over different final rotational levels:

$$\frac{{\rm d}\sigma^s}{{\rm d}\Omega} = \sum_{J'\tau'}\frac{{\rm d}\sigma}{{\rm d}\Omega}(J\tau \to J'\tau'). \tag{15}$$

The corresponding integral cross-section in the lab frame can be computed as

$$Q_e^{\rm LF} = \sigma_{rd}^{\rm B} + \sigma_{cc} - \sigma_{fd}^{\rm B}. \tag{16}$$

The individual term on the right-hand side refers to the integral cross-sections computed within Born approximation for a rotating dipole, in the fixed nuclei (FN) approximation after solving the close-coupling equations and cross-sections for a fixed dipole.

In the same framework, the MTCS are also written as

$$\sigma_M = \sigma^{\mathrm{B}}_{M(rd)} + \sigma_{M(cc)} - \sigma^{\mathrm{B}}_{M(fd)}, \tag{17}$$

where the meanings of the symbols are the same as defined for integral cross-sections and subscript M refers to MTCS. This scheme is implemented in POLYDCS [46] and is employed to obtain DCS in the present study.

2.2 *Total cross-section*

The total electron scattering cross-sections (Q_{T}) are needed in many areas of applied physics. These can be measured accurately by using the linear transmission apparatus [50,51]. Q_{T} also serve as checks on other cross-sections determined theoretically. Q_{T} in any given scattering process is the sum of the elastic and inelastic contributions to electron–molecule interaction phenomenon.

$$Q_{\mathrm{T}} = Q_e + \sum_{n\to n'} Q_{ee} + Q_i + \sum_k Q_k, \tag{18}$$

where Q_e, Q_{ee}, Q_i and Q_k refer to integral elastic, summed electronic excitation, ionisation and other inelastic types of cross-sections like dissociation, dissociation-attachment cross-sections respectively. The summed excitation cross-sections include contributions from dipole and non-dipole excited states. The electron attachment and vibrational cross-sections, being very small in the present energy domain, are ignored in the present calculations. In the energy regions lower than the ionisation threshold, only the elastic and electronic excitations contribute to total cross-sections. Q_{ex} are obtained from R-matrix approach and Q_i are determined using the BEB model.

3. Methodology and computational details

The geometry of targets was referred from NIST [1] and optimised at HF level employing the $D95^{**}$ basis sets using GAUSSIAN 03 [52]. The scattering calculations were then performed using the SCE and R-matrix approaches.

The molecular electron density and potentials in SCE formalism were computed using SCELiB code [53]. The upper limit of the angular momentum for the bound-state wave functions was kept at 50 to ensure a good convergence of molecular properties. The radial step for integration was kept to a fixed mesh with a step size of 0.001 a.u. The quadrature grid was chosen to obtain normalised wave functions. These normalised wave functions yielded a reasonably good HF value of dipole moment for each molecular system. The scattering calculations were then performed using POLYDCS code. Sufficient number of partial waves were considered in the scattering problem to achieve satisfactory convergence in cross-sections. The scattering results are discussed in the next section. The total cross-sections in intermediate to high energy range is approximated by the sum of elastic, ionisation and electronic excitation cross-sections. The low-energy scattering calculations within the fixed-nuclei approximation are based on the R-matrix method. The nuclei was assumed to be stationary at the ground-state equilibrium geometry of the molecule. The self-consistent field (SCF) procedure is used to generate molecular orbitals. The ground-state trial wave function of the scattering system consists of only the ground state in the static exchange (SE) model. This model is unique in which the target electrons are not allowed to move among the virtual orbitals, thus producing a single configuration. The extra incoming electron is then allowed to occupy any virtual orbital for a particular irreducible representation of the scattering state. Several excited states are included in addition to the molecular ground state through the use of close coupling (CC) expansion. The complete active space (CAS) is created where valence bound molecular orbitals are excited to a few unoccupied molecular orbitals. In CAS-CI model, excited states below 10 eV were included in the ground-state wave function for each molecular system. This model provides both the elastic and electronic excitation cross-sections and is best suited to obtain the scattering results. The CAS-CI calculations were done using the UKRmol+ (version 1.0) codes taking the boundary radius as $12a_0$. The R-matrix cross-sections contain contributions from only a few partial waves (upto $l = 4$). Further, the partial wave expansion does not converge in the FN approximation for polar molecules. This lack of convergence is circumvented by means of a Born correction by invoking Born top-up closure formula. The works cited in refs [12–15] can be referred for further details. The implications of long-range effects in electron scattering by polar molecules have also been discussed in a review article [49]. The relevant information about the targets and the scattering model is given in tables 1 and 2 respectively.

4. Results and discussion

In this section, the SCE-based results are reported beyond the ionisation threshold. This includes DCS, ICS and MTCS. The present results are also compared with

Table 1. Ground-state target parameters.

Molecule	Point group	Number of e^-	Ionisation energy (eV)	Dipole moment (ea_0)	Number of states included in CAS-CI model
O_3	C_{2v}	24	12.53[1], 13.37[2]	0.209[1] (0.26)	24
OSO	C_{2v}	32	12.35[1], 13.46[2]	0.641[1] (0.83)	24
SOS	C_{2v}	40	9.22[2,3]	0.331[3] (0.34)	24
S_3	C_{2v}	48	9.68[1], 9.77[2]	0.220 (0.30)	24

[1]Experimental value [1].
[2]Theoretical value.
[3]GAUSSIAN.
Figures in parenthesis indicate HF values obtained in SCE formalism.

Table 2. Modelling parameters.

Molecule	HF configuration[1]	Active space[2]	Number of target states per IR in CAS-CI model		Total number in CAS-CI model
			Singlets	Triplets	
O_3	(6,1,4,1)	(7,2,5,1)	3	3	24
OSO	(8,2,5,1)	(9,3,6,1)	3	3	24
SOS	(9,2,7,2)	(10,6,8,2)	3	3	24
S_3	(11,3,8,2))	(12,4,9,2)	3	3	24

[1]HF configuration (6,1,4,1) means 6 bound orbitals of A_1, 1 of B_1, 4 of B_2, 1 of A_2.
[2]Active space (7,2,5,1) means 7 virtual orbitals of A_1, 2 of B_1, 5 of B_2, 1 of A_2.

the available data. This is followed by *R*-matrix results. Finally, the cross-sections are reported over the energy range of 0.1 to 5 keV.

O_3 and S_3: Ozone is a highly relevant atmospheric gas and has consumer applications. Apart from protecting the life from exposure to harmful radiation reaching the Earth's atmosphere, it is used to control bacterial growth in food storage units, clean air, disinfect drinking water etc. Thus, it is pertinent to produce ozone efficiently in industrial applications. This requires a better understanding of synthesis mechanisms in gaseous discharges [2,3] and the electron–molecule interactions. Ozone being a chemically reactive species [54], the present theoretical results would be useful in providing cross-section data. Pablos *et al* [55] have experimentally studied the electron impact collision with ozone to obtain total cross-sections from 300 eV onwards. These results have an error of $\pm 10\%$. This is the only available TCS data in the high-energy region. These authors have further validated their observations by performing theoretical scattering studies based on independent-atom-model (IAM). Joshipura *et al* [56] have employed additivity rule to obtain ionisation and total cross-sections from 30 to 3000 eV range using the complex optical potential method.

Shyn and Sweeney [57] have measured differential elastic scattering cross-sections of ozone by electron impact using crossed beam method. The energy and angular range measured were from 3.0 to 20 eV and from 12 to 156°, respectively. The DCS data were extrapolated to find missing angle data. This enabled one to compute integral and momentum transfer cross-section data. Lee *et al* [17] and Bettega *et al* [18] have reported results from an *ab-initio* calculation of low-energy electron scattering upto 30 eV. Lee *et al* have reported a theoretical study of elastic electron–ozone collisions in the 3–80 eV energy range. These calculations were carried out in a FN approximation at the ground-state equilibrium geometry of ozone. The Schwinger variational iterative method is used to calculate the low partial wave scattering amplitudes at the SE level. The higher partial wave contributions were taken into account through a Born-closure procedure using a point dipole potential. Their results compared extremely well with the available experimental and theoretical data in the literature. Bettega *et al* applied the Schwinger multichannel method with pseudopotentials to compute elastic integral, differential and momentum transfer cross-sections in an energy range from 6 eV to 30 eV. The scattering results of Sarpal *et al* [16] were compared by one of the present author earlier using the *R*-matrix based study [12]. Their results were in agreement and hence are not shown in the graphs.

The elastic DCS obtained for electron scattering from O_3 are plotted at different energies in figures 1–4. At small scattering angles, the DCS rises steeply due to the long-range scattering caused by its dipole field ($\mu = 0.209$ a.u.). The sharp dip around 100° signi-

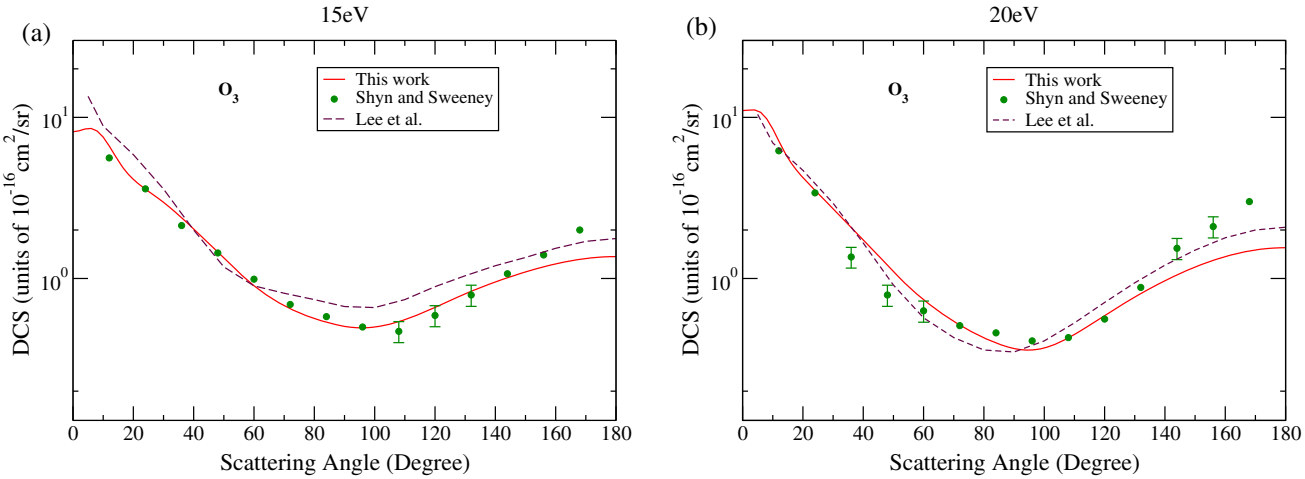

Figure 1. Elastic DCS of O_3 at (**a**) 15 eV and (**b**) 20 eV. Solid lines indicate this work, double dashed lines indicate the work of Lee *et al* and circles indicate the work of Shyn and Sweeney.

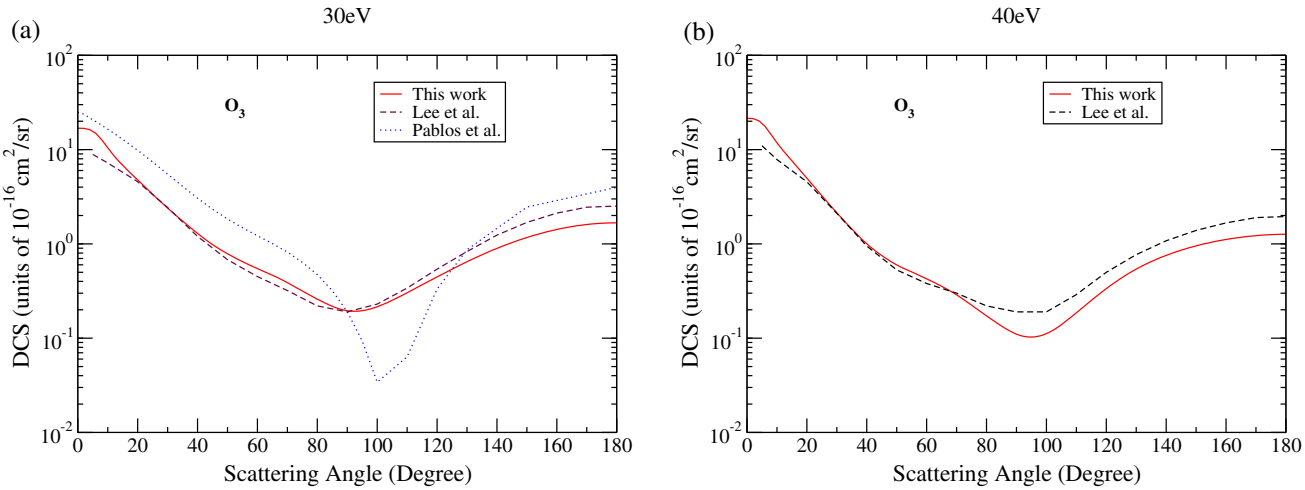

Figure 2. Same as figure 1 but at 30 eV and 40 eV. Solid lines indicate this work, double dashed lines indicate the work of Lee *et al* and dotted lines indicate the work of Pablos *et al*.

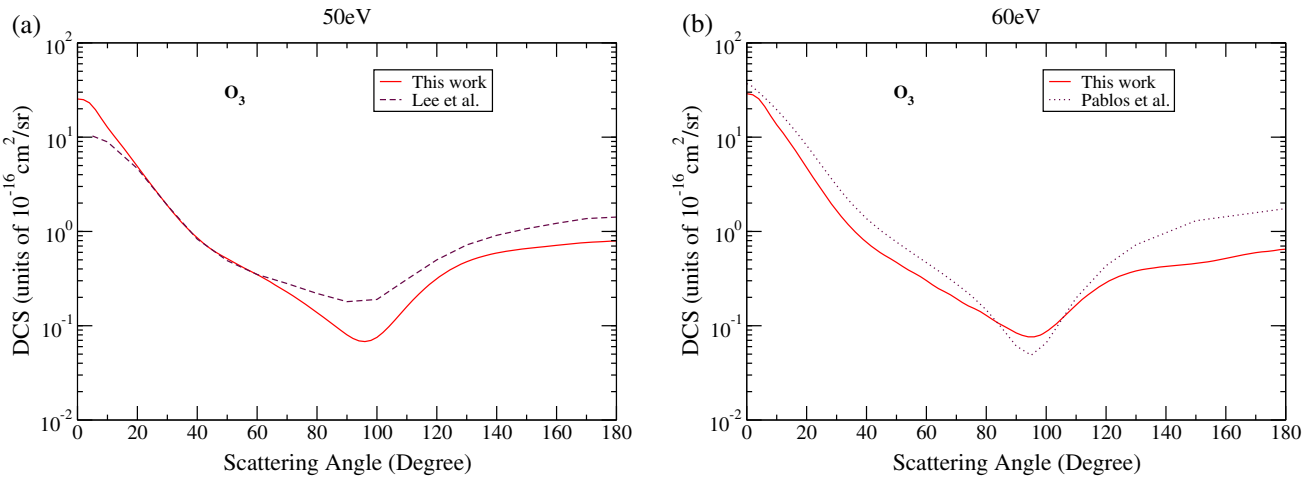

Figure 3. Elastic DCS at (**a**) 50 eV and (**b**) 60 eV. Solid lines indicate this work; dashed lines indicate the work of Lee *et al* and dotted lines indicate the work of Pablos *et al.*

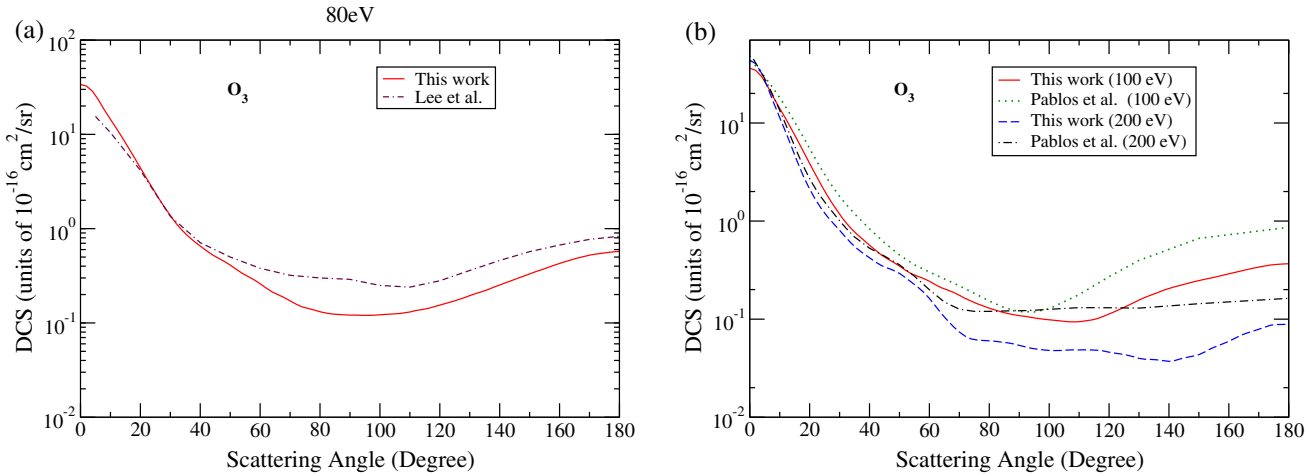

Figure 4. Elastic DCS at (**a**) 80 eV, (**b**) 100 eV and 200 eV. Solid and dashed lines indicate this work, dashed dotted lines indicate the work of Lee *et al* and dotted and dashed dotted lines indicate the work of Pablos *et al.*

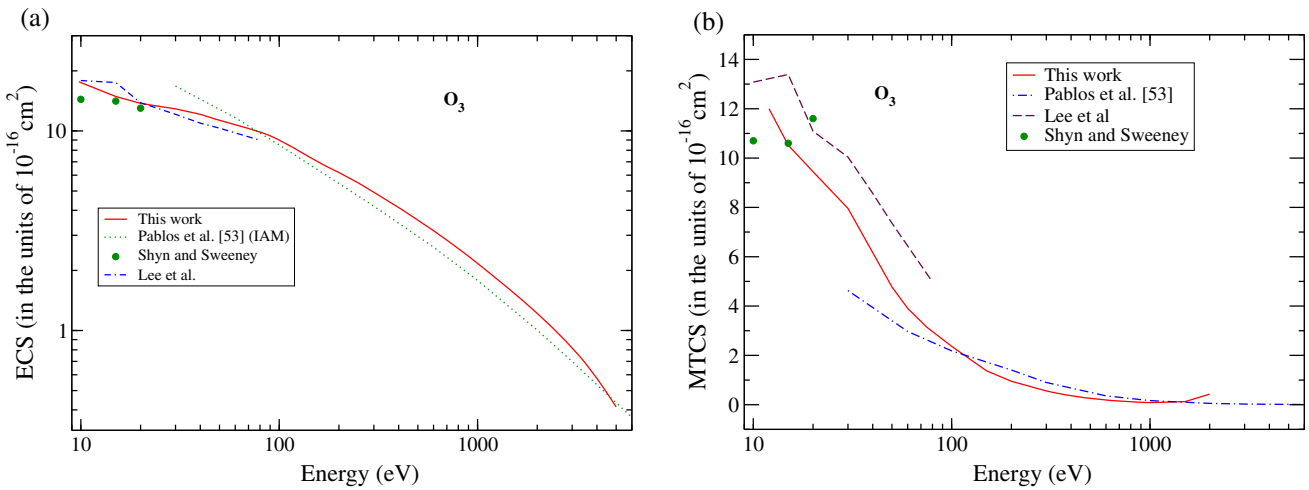

Figure 5. Cross-sections for e^- scattering from O_3. (**a**) Elastic: solid line, this work; dotted line, Pablos *et al* (IAM); dashed dotted lines, Lee *et al*; circles, Shyn and Sweeney, (**b**) MTCS: solid line, this work; dotted dashed line, Pablos *et al* (IAM); dashed line, Lee *et al*; circles, Shyn and Sweeney.

fies the dominance of p-wave. At angles greater than 100°, the DCS increases with increasing angle which implies that backward scattering is significant. The overall shape and behaviour of the present DCS across the entire energy range is consistent with the experimental results of Shyn and Sweeney and other theoretical calculations.

The SCE-based elastic and momentum transfer cross-sections are plotted in figures 5a and 5b respectively. We find an extremely good agreement between the present and other calculations. The present MTCS are in excellent agreement with the results of Pablos *et al*. The results of Lee *et al* systematically lie above the present results at all the energies.

The molecular structure of S_3 is the same as ozone except that it has an extra neon core. This molecule occurs naturally on Venus and Jupiter-Io atmosphere [6]. Our present and past studies [13] provide the only collision data for this molecule. The elastic DCS at various energies are plotted in figure 6a between 30 and 100 eV and there is more than one minima. The steep fall in DCS at small angles is a reflection of its polar nature. As the energy of the projectile increases from 30 to 200 eV, the magnitude of DCS at low scattering angles decrease. The peak is around 95° at 30 eV whereas the minimum occurs around 105°. In between these energy intervals, there are small undulations due to the effect of interference among various partial waves of high angular momenta. The integral elastic and momentum transfer cross-sections are plotted in figure 6b. These cross-sections decrease monotonically with the increase in projectile energy.

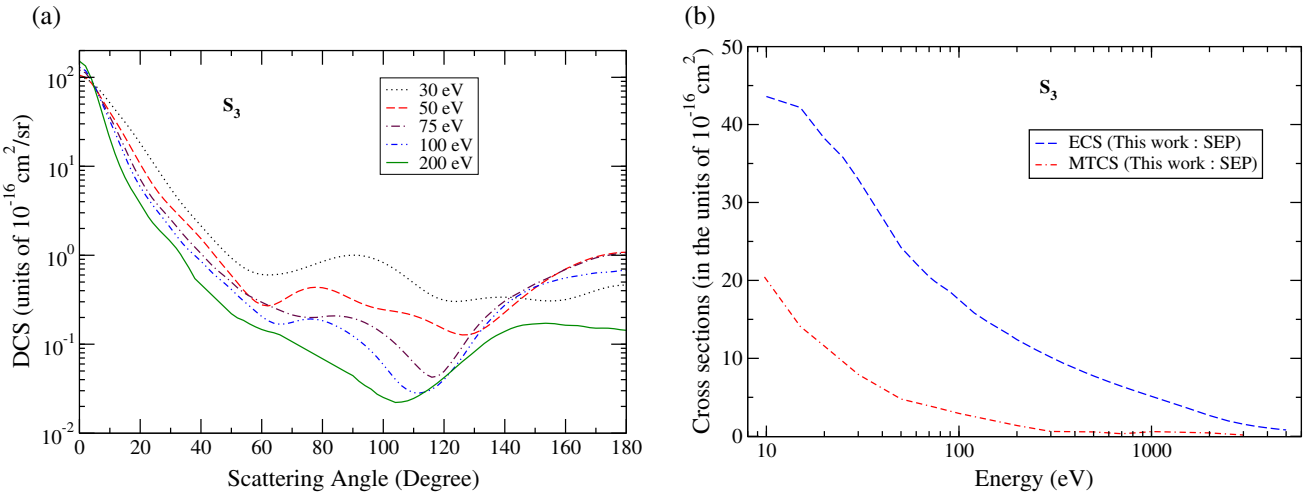

Figure 6. Cross-sections for e^- scattering of S_3. (**a**) Elastic DCS at 30 eV; dotted lines, 50 eV; dashed lines, 75 eV; dashed dotted lines, 100 eV; double dotted dashed lines and 200 eV; solid lines. (**b**) ECS; dashed lines and MTCS; dashed dotted lines.

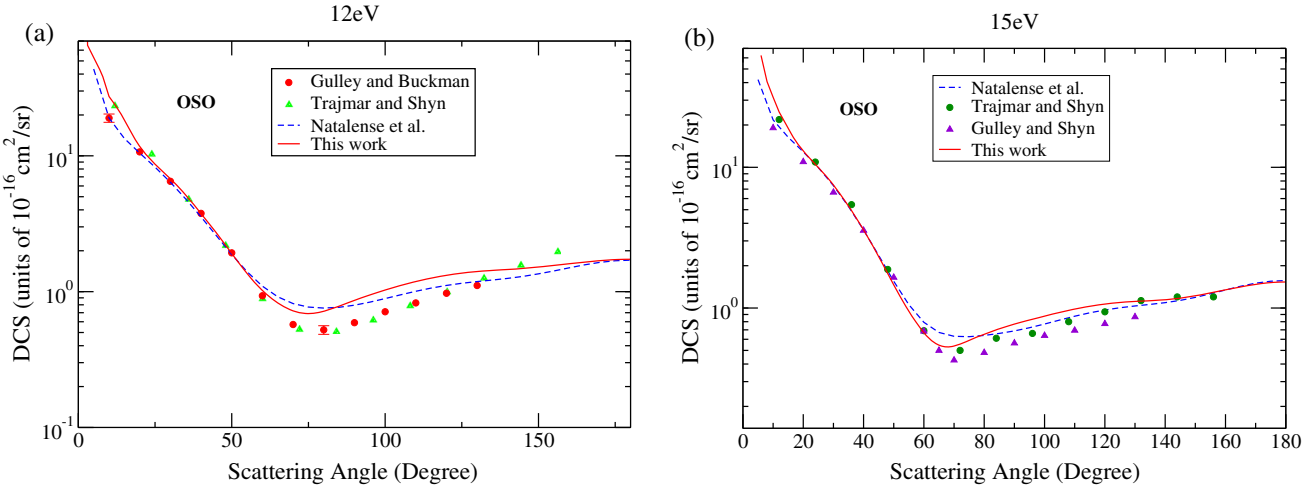

Figure 7. Elastic DCS for e^- scattering from OSO at (**a**) 12 eV and (**b**) 15 eV. Solid lines indicate this work, dashed lines indicate the work of Natalense *et al*, circles indicate the work of Trajmar and Shyn and triangles indicate the work of Gulley and Buckman.

OSO and SOS: The OSO and SOS also form a set of isovalent molecules of O_3 where the O atom(s) is (are) replaced by the S atom(s). Both these molecules are astrophysically relevant [58–60]. The e^- interactions with OSO play a role in combustion, planetary atmosphere, diffuse-discharge switches, plasma-assisted treatment of biocompatible materials and biomedical surfaces [61–63]. Machado *et al* used the relative flow technique to measure elastic DCS in the angular range 5–130°. Trajmar and Shyn [64], Gulley and Buckman [65] obtained DCS in the angular range 12–168° and 10–130° respectively using the crossed electron beam. Natalense *et al* [19] obtained rotationally summed and rotationally inelastic differential, integral and momentum transfer cross-sections for electron scattering in the 3–30 eV impact energy range. These calculations were performed by employing Schwinger multichannel method with pseudopotentials in SE approximation. The long-range effects on the scattering cross-sections due to the permanent dipole nature of the target were included within the first Born approximation. Gianturco *et al* [66] implemented SCE approach to obtain integral and differential cross-sections for the elastic process. Their calculations were restricted to 30 eV. The dipole effects on scattering were accounted using the multipole-extracted adiabatic nuclei approximation.

The present elastic DCS results are plotted in figures 7–10 at different energies. The overall shape of the present elastic DCS at different energies compares

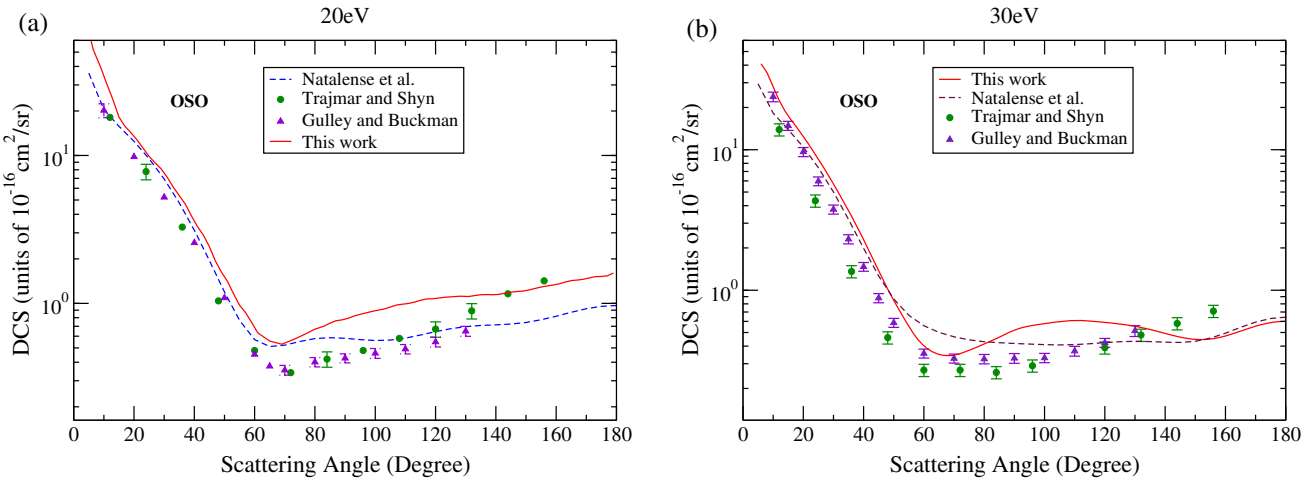

Figure 8. Elastic DCS for e^- scattering of OSO at (**a**) 20 eV and (**b**) 30 eV. Solid lines indicate this work, dashed lines indicate the work of Natalense *et al*, circles indicate the work of Trajmar and Shyn and triangles indicate the work of Gulley and Buckman.

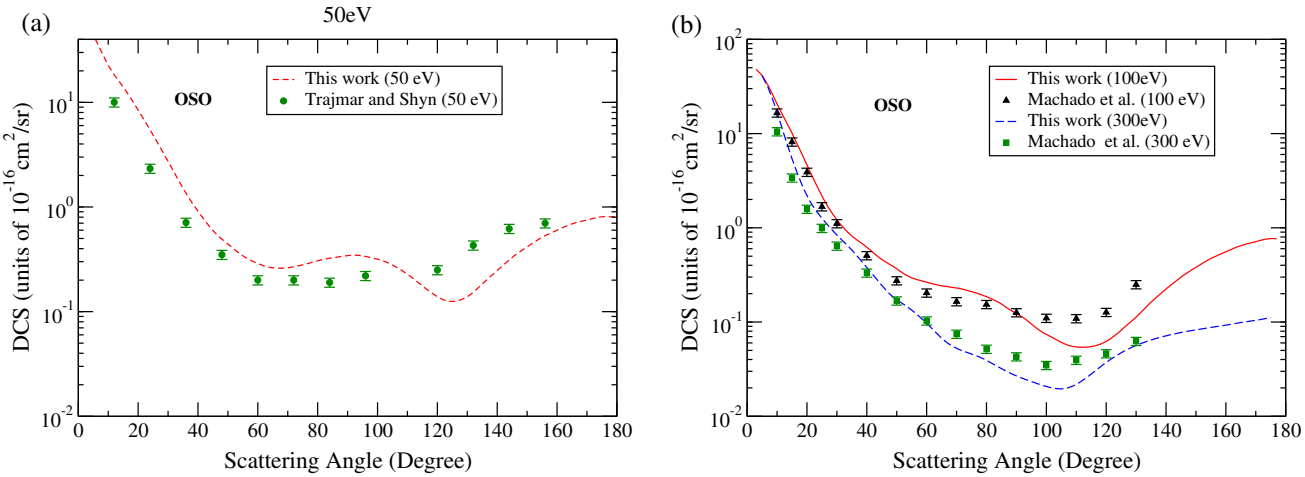

Figure 9. Elastic DCS for e^- scattering of OSO at (**a**) 50 eV and (**b**) 100 eV and 300 eV. Solid and dashed lines indicate this work, circles indicate the work of Trajmar and Shyn, triangles and squares indicate the work of Machado *et al.*

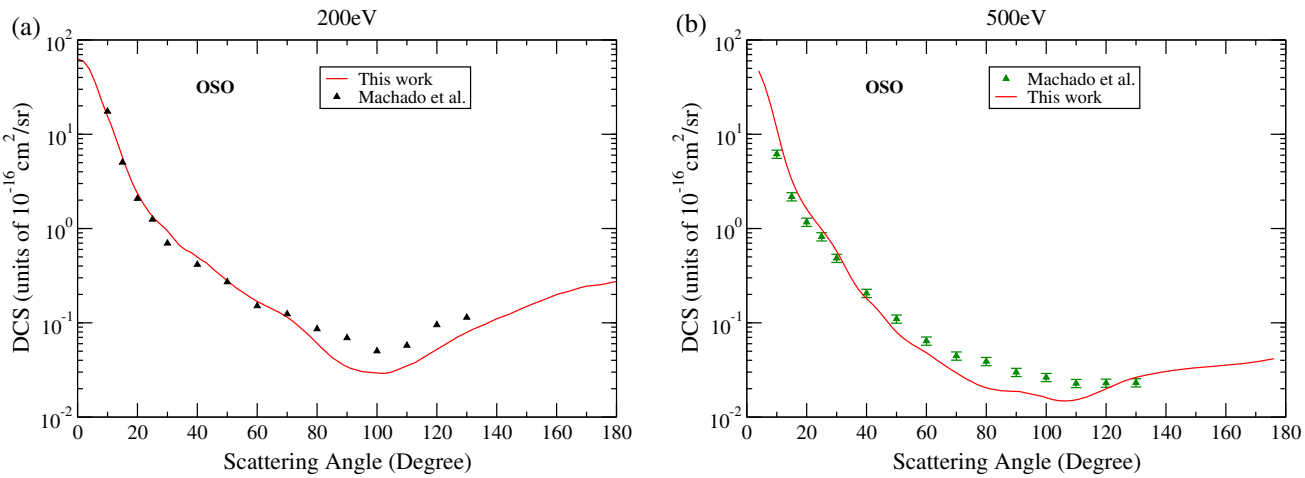

Figure 10. Elastic DCS for e^- scattering of OSO at (**a**) 200 eV and (**b**) 500 eV. Solid line indicates this work and triangles indicate the work of Machado *et al.*

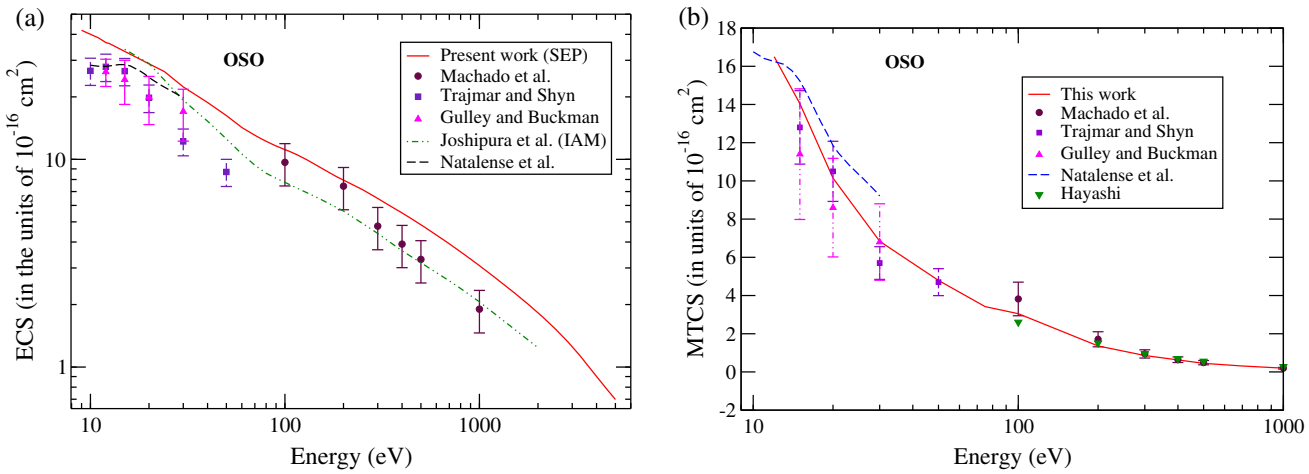

Figure 11. Cross-sections for e^- scattering of OSO. (**a**) ECS and (**b**) MTCS. Solid lines indicate his work, double dotted dashed line indicates the work of Joshipura *et al*, dashed lines indicates the work of Natalense *et al*, triangles indicate the work of Gulley and Buckman, squares indicate the work of Trajmar and Shyn, circles indicate the work of Machado *et al.* and inverted traiangles indicate the work of Hayashi.

well with the experimental results of Trajmar and Shyn [64], Gulley and Buckman [65] and Machado *et al.* The present results are in excellent agreement with *ab-initio* calculations and experimental data at 12 to 30 eV. At higher energies, the agreement is still satisfactory.

Joshipura and Gangopadhyay [67] used theoretical complex scattering potential model to obtain elastic, total and grand total cross-sections. They have accounted the long-range interactions due to the polar nature by including the rotational cross-sections separately to total cross-sections (summed elastic and inelastic) to obtain grand total cross-sections. Hence, their elastic cross-sections ought to be lower than ours. The present SEC results are consistent with the experimental data. Vinodkumar *et al* [68] performed low-energy calculations using *R*-matrix formalism through the Quantemol-N package. The high-energy calculations were done using the IAM-based SCOP model.

Q_e and Q_m are displayed in figures 11a and 11b respectively. The present Q_e values are within the experimental errors of other workers' results even at energies as low as 15 eV. The present Q_e values at 400, 500 and 1000 eV lie a little above the results of Machado *et al.* The MTCS are in good agreement with the experimental values of Machado *et al*, Trajmar and Shyn, Gulley and Buckman and Hayashi [69]. The MTCS of Natalense *et al* are higher than the present results.

Like S_3 there is no other electron–SOS collision study available to date other than our earlier work. The elastic DCS for SOS are reported in figure 12a, while both Q_e and Q_m are shown in figure 12b. The Born-corrected DCS displays oscillatory behaviour beyond 40° at high energies. This oscillatory behaviour is a characteristic of the lack of convergence of the partial wave contributions originating from the subtraction term $A_L^B P_L(\cos\theta)$; the quantity calculated under Born approximation in POLY-DCS. This oscillatory behaviour can partly be reduced provided the Born correction is applied by augmenting the T-matrices [70,71].

The SCE results presented in figure 13a for all the targets show a trend in elastic cross-sections at different energies. Beyond the ionisation threshold, the scattering process is clearly dominated by the geometrical size of the target.

The CAS-CI *R*-matrix scattering calculations have already been performed for these isovalent molecules [12–15], where a good agreement was observed between the CAS-CI results and other theoretical and experimental results. In these studies, resonances were also characterised. However, the calculations were restricted to around 10 eV energies. The CAS-CI results are referred in the present work to evaluate how these cross-sections compare with the present SCE cross-sections at ionisation threshold and to estimate cross-sections from low to high energy region. The important aspects related to the target and scattering modelling like HF configuration, number of states included in CAS-CI, active space considered are mentioned in table 2. The CAS-CI results are displayed in figure 13b. The dipole moment dominates the scattering process in this energy domain.

Encouraged by the good quality of the present SCE and the CAS-CI *R*-matrix results, the elastic and MTCS obtained from these approaches were evaluated near the ionisation threshold. These cross-sections were found to vary smoothly near the ionisation potential for all the targets. The results are displayed in figures 14 and

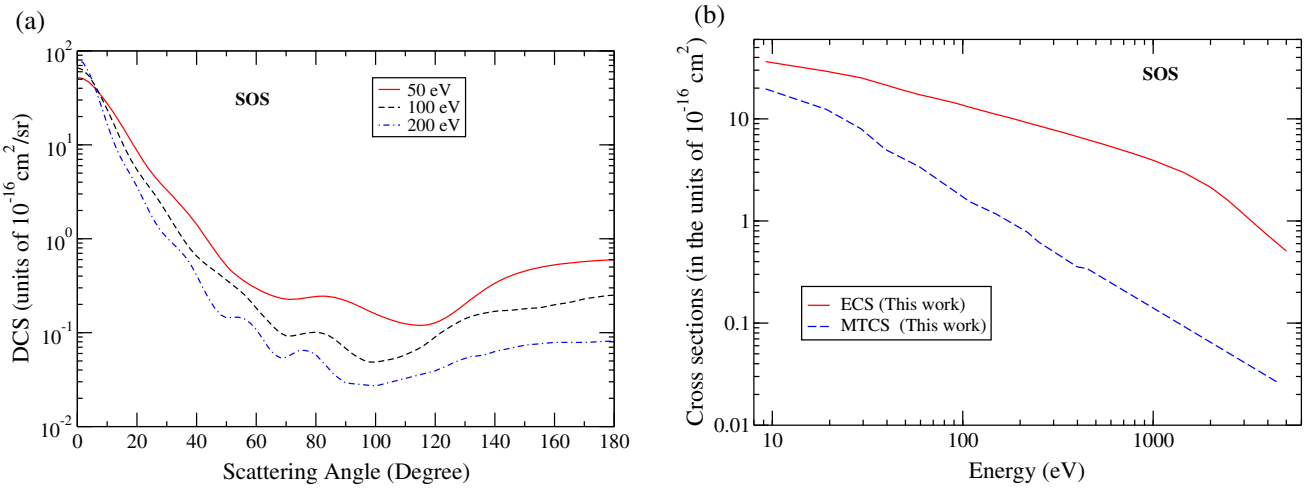

Figure 12. Cross-sections for e^- scattering of SOS. (**a**) Elastic DCS at 50 eV (solid line), 100 eV (dashed line) and 200 eV (double dotted dashed line) and (**b**) ECS (solid line) and MTCS (dashed line).

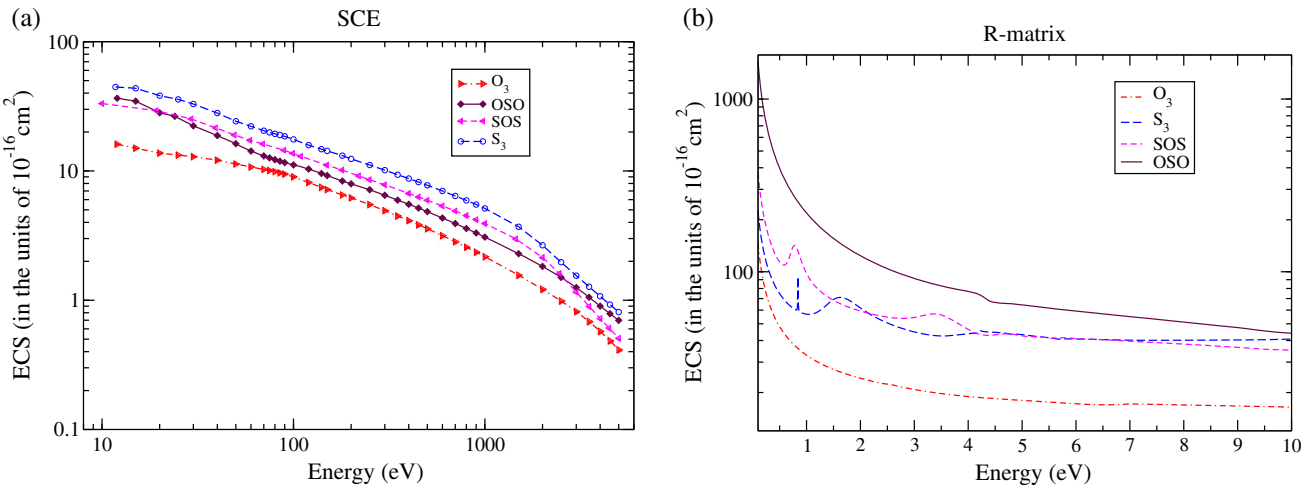

Figure 13. ECS for isovalent molecules. (**a**) SCE formalism (this work) and (**b**) CAS-CI R-matrix.

15 from 0.1 to 5 keV. The comparative evaluation is also made in table 3. It can be easily concluded that the amalgamation of theories of different types can describe the electron scattering process satisfactorily over a wide range of energy values.

The present SCE approach can only account for elastic cross-sections. The inelastic cross-sections are also required to obtain the total cross-sections. Q_{ee} were obtained using CAS-CI model whereas the ionisation cross-sections were obtained using the BEB model.

Q_i for all targets plotted from the ionisation threshold up to 5 keV are shown in figure 16a. The experimental value of ionisation potential was used in calculation to ensure the correct threshold behaviour. The present BEB results were overlapping with the results of Kim *et al* [72]. The numerical values of BEB cross-sections are given in NIST website [73]. For the sake of brevity, we

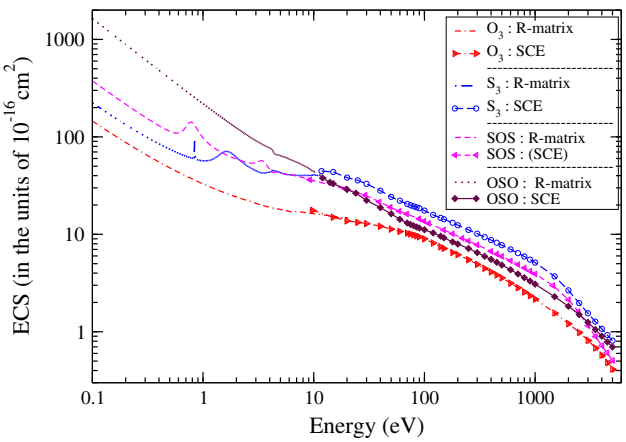

Figure 14. ECS for the isovalent molecules from the amalgamation of R-matrix and SCE formalisms.

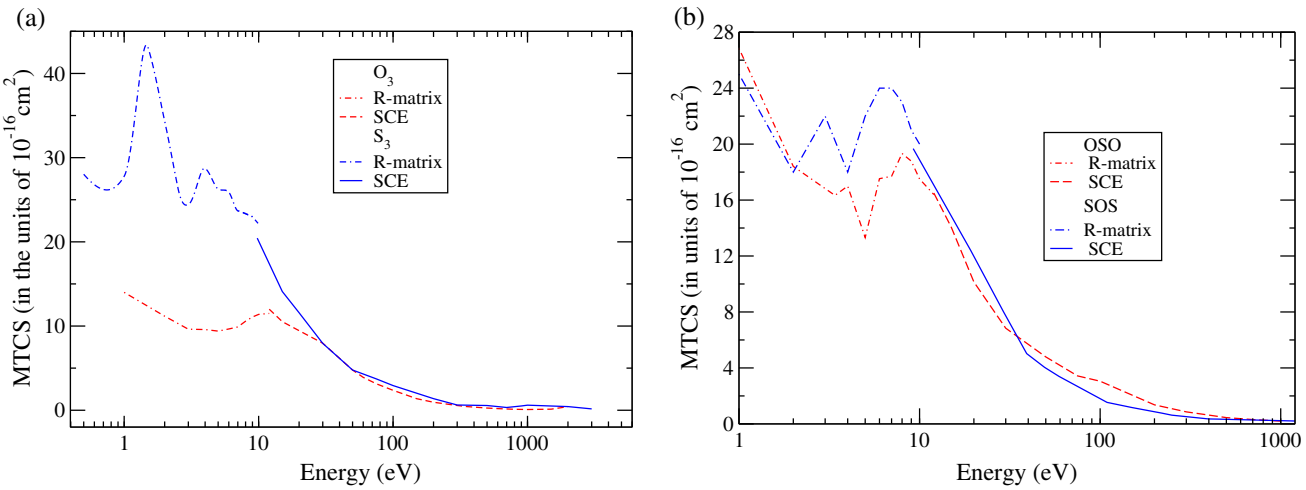

Figure 15. MTCS obtained from *R*-matrix and SCE for (**a**) O_3 (double dotted dashed and dashed lines) and S_3 (dashed dotted and solid lines). (**b**) OSO (double dotted dashed and dashed lines) and SOS (dashed dotted and solid lines).

Table 3. Evaluation of *R*-matrix and SCE cross-sections (10^{-16}cm^2) near the ionisation threshold.

Molecule	Energy (eV)	*R*-matrix ECS	SCE ECS	Energy (eV)	*R*-matrix MTCS	SCE MTCS
O_3	12	15.98	16.12	12	11.5	12
S_3	10	40.76	43.6	10	22.2	20.25
OSO	12	38.0	36.5	12	16.39	16.5
SOS	10	35.17	35.8	10	20	19

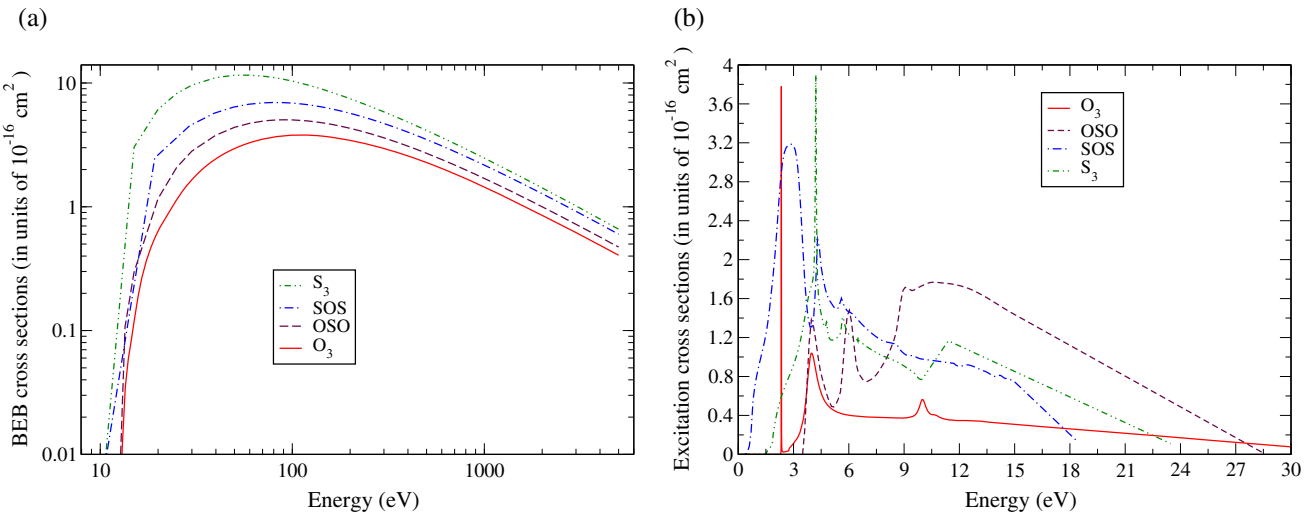

Figure 16. Inelastic cross-sections of isovalent targets. (**a**) BEB ionisation and (**b**) electronic excitation.

have not shown BEB results of Kim *et al*. The ionisation cross-sections show $\log E/E$ behaviour at higher energies.

In figure 16b, we have plotted the summed electronic excitation cross-sections for different targets from 0.1 to 25 eV. These cross-sections include the contributions from discrete spin-allowed and spin-forbidden transitions. Q_{ee} of a particular target depends upon the transition moment and its excitation threshold. The higher excitation thresholds results in smaller excitation cross-sections. Both the excitation and ionisation cross-sections increase steeply from the threshold energy to a maximum value and then start decreasing with further increase in the projectile energy. However, the maxi-

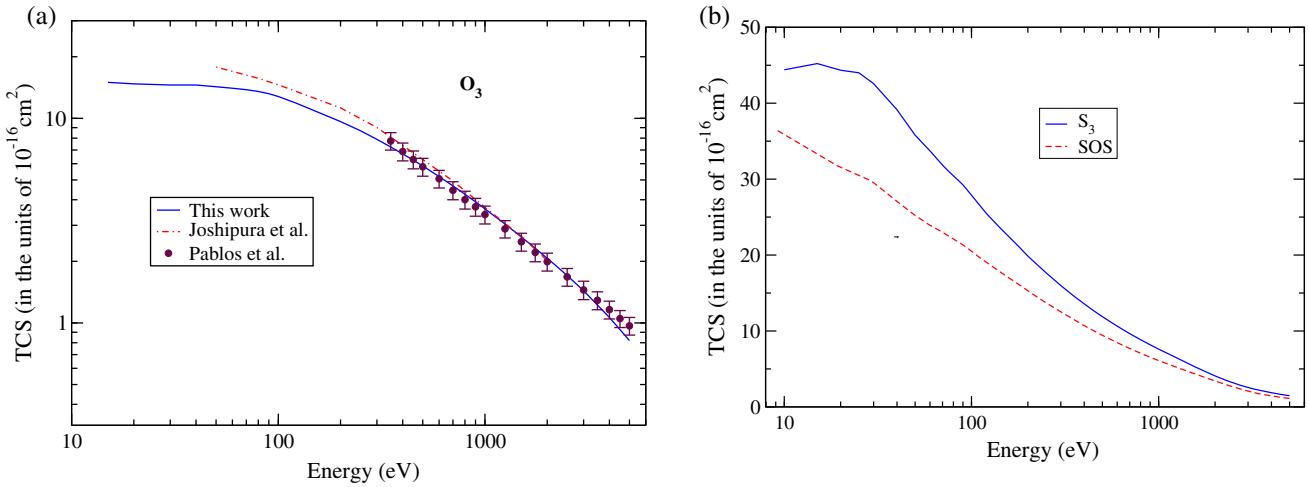

Figure 17. TCS for (**a**) O_3: solid line indicates this work, dashed double dotted line indicates Joshipiura *et al*, circles indicate Pablos *et al* and (**b**) S_3 (solid line; this work) and SOS (dashed double dotted line; this work).

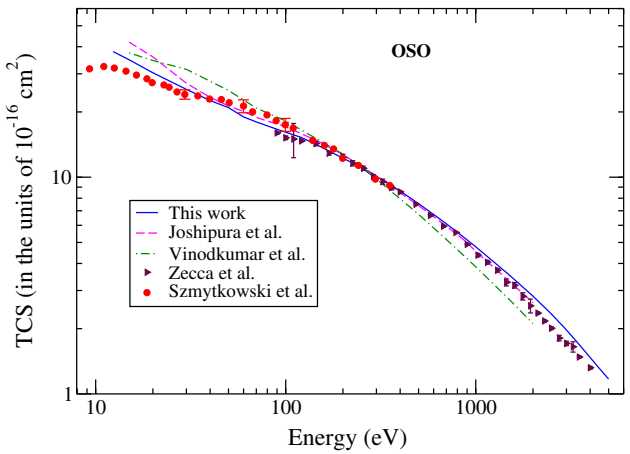

Figure 18. TCS for OSO. Solid line indicates this work, dashed line indicates the work of Joshipura *et al*, dashed dotted line indicates the work of Vinodkumar *et al*, triangles right indicates the work of Zecca *et al* and circles indicate the work of Szmytkowski *et al.*

mum of Q_{ee} lies near the excitation threshold whereas for ionisation process it is between 80 and 100 eV energy range for the present targets. The fall in Q_{ee} is sharp near the ionisation threshold. These trends are evident from figures 16a and 16b in Q_i and Q_{ee}. Since cross-sections represent the probability of a particular process to occur, it means that at energies less than the ionisation threshold, excitation phenomenon is dominant whereas beyond the ionisation threshold, the ionisation phenomenon becomes more probable than the excitation. Q_T obtained by summing SCE elastic and other inelastic cross-sections are displayed in figures 17 and 18. The experimental and theoretical data of total cross-section is available for O_3 and OSO only. The present Q_T shown in figure 17a for O_3 are in good accord with the experimental data of Pablos *et al* and theoretical data of Joshipura *et al.* The results for S_3 and SOS are displayed in figure 17b.

The present Q_T for OSO are plotted in figure 18 where they are also compared with the experimental results of Zecca *et al* [74] and Szmytkowski *et al* [75] and theoretical results of Joshipura and Gangopadhyay [67], Vinodkumar *et al* [68]. The maximum variation was about 10% for both O_3 and OSO. However, the present results are within their experimental uncertainties. Like Q_e and Q_m, Q_T obtained from the R-matrix and SCE vary smoothly near the ionisation potential for all the targets. These results are displayed in figure 19.

Some important inferences are drawn from the study of electron interactions with the isovalent molecules studied here. It is well known that molecular properties like dipole moment and dipole polarisability affect the scattering dynamics and therefore the scattering cross-sections. However, there is no definite trend in these properties for isovalent molecules (table 1). Except for OSO, all the other three target molecules have dipole moments in the range between 0.2 and 0.3 a.u. OSO has a reasonably large value of dipole moment (0.641 a.u.) among all the isovalent molecules. S_3 has a dipole polarisability (isotropic) of $68a_0^3$ which is much larger than the other targets.

(i) It is the long-range dipole interaction and not the geometrical size of molecule which dominates scattering process in the low-energy region. This explains the reason why SOS has larger Q_e and Q_T than S_3 in spite of its smaller geometrical size.
(ii) The polarisation effects are important in low-energy domain, but get suppressed even by

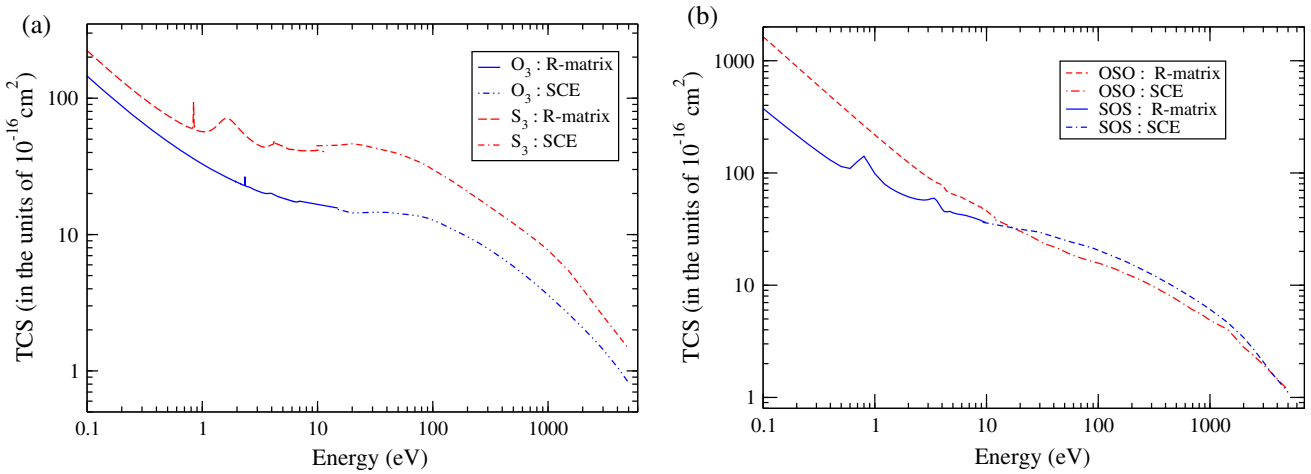

Figure 19. TCS obtained from two formalisms and (**a**) O_3 and S_3 and (**b**) OSO and SOS.

weakly polar molecule. It would certainly be interesting to extend the scattering studies from non-polar molecules to evaluate the dependence of polarisation in low energy range.

(iii) The trends in the cross-sections beyond ionisation threshold are influenced by the geometrical size of the molecules.

(iv) The present approach is simple and is capable of providing reliable estimates of TCS.

(v) The amalgamation of *R*-matrix and SCE approaches can be used the estimate the collision cross-sections over a wide energy range.

5. Conclusions

We have carried out close coupling calculations at CI level using the UKRmol+ codes below the ionisation threshold of all target molecules. The SCE-based calculations are performed from the ionisation threshold upto 5 keV. In the energy range of the present study, the ionisation cross-sections contribute significantly to total scattering cross-sections. The dipole and polarisation effects are less pronounced in this region unlike low-energy region. The total cross-section values obtained by incoherently adding the inelastic and the integral elastic cross-sections are very close to the experimentally measured total cross-sections in the case of O_3 and OSO for which the collision data are available. The other cross-sections like differential, elastic and momentum transfer also show excellent agreement with the available works. Both formalisms exhibit smooth behaviour in CS near the ionisation energy. The present study confirms the validity of our model that enables us to predict the cross-sections from 0.1 to 5 keV. The dependence of cross-sections on the dipole moment is explained in low- and high-energy regions. It dominates the geometric size of the molecule only in the low-energy energy range. Beyond the ionisation threshold, the trends in the cross-sections are governed by the geometrical shape of the molecule. These observations would not have been possible had the scattering been studied from a single molecule.

NOTE: The codes were downloaded from ccpforge website http://ccpforge.cse.rl.ac.uk/gf/project/ukrmol-in. This site has shut down since 2019. The updated versions of UKRmol+ codes are available on Zenodo [76].

Acknowledgements

The author AB is thankful to Prof. Robert Lucchese, Department of Chemistry, Texas AM University for his guidance on single centre expansion method and to Dr Fernando R Clemente, Gaussian Inc for giving useful insights about GAUSSIAN-16 during the workshop held in New Delhi from January 8 to 12, 2018.

References

[1] http://cccbdb.nist.gov
[2] B Elliasson and U Kogelschatz, *J. Phys. B* **19**, 1241 (1986)
[3] P Pignolet, S Hadj-Ziane, B Held, R Peyrous, J M Benas and C Coste, *J. Phys. D* **23**, 1069 (1990)
[4] J R Spencer, K L Jessup, M A McGrath, G E Ballester and R Yelle, *Science* **288**, 1208 (2000)
[5] S Thorwirth, M C McCarthy, C A Gottlieb, P Thaddeus, H Gupta and J F Stanton, *J. Chem. Phys.* **123**, 054326 (2005)
[6] J S Lewis, *Physics and chemistry of the solar system* (Academic Press, 2004)

[7] L E Machado, R T Sugohara, A S dos Santos, M-T Lee, I Iga, G L C de Souza, M G P Homem, S E Michelin and L M Brescansin, *Phys. Rev. A* **84**, 032709 (2011)
[8] W J Lo, Yu-J W, and Y-P Lee, *J. Chem. Phys*. **117**, 6655 (2002)
[9] Y Itikawa, *Molecular processes in plasmas collisions of charged particles with molecules* (Springer, 2007)
[10] L G Christophorou and J K Olthoff, *Fundamental electron interactions with plasma processing gases* (Springer, 2004)
[11] B Bederson and H Walther, *Adv. in atomic, molecular and optical physics* (Academic Press, 2000) Vol. 43
[12] M Gupta and K L Baluja, *J. Phys. B* **38**, 4057 (2005)
[13] S Kaur, A Bharadvaja and K L Baluja, *Phys. Rev. A* **83**, 062707 (2011)
[14] S Kaur and K L Baluja, *Phys. Rev. A* **82**, 022717 (2010)
[15] M Gupta and K L Baluja, *Phys. Rev. A* **73**, 042702 (2006)
[16] B K Sarpal, B M Nestmann and S D Peyerimhoff, *J. Phys. B: At. Mol. Opt. Phys.* **13**, 1333 (1998)
[17] M T Lee, S E Michelin, T Kroin and L E Machado, *J. Phys. B: At. Mol. Opt. Phys.* **31**, 1781 (1998)
[18] M H F Bettega, M T do N Varella, L G Ferreira and M A P Lima, *J. Phys. B: At. Mol. Opt. Phys*. **31**, 4419 (1998)
[19] A P P Natalense, M T do N Varella, M H F Bettega, L G Ferreira and M A P Lima, *J. Phys. B: At. Mol. Opt. Phys*. **32**, 5523 (1999)
[20] P G Burke, *R-Matrix theory of atomic collisions: Application to atomic, molecular and optical processes* (Springer-Verlag, Berlin, 2011)
[21] J Tennyson, *Phys. Rep.* **491**, 29 (2010)
[22] D Madden, J Tennyson and R Zhang, *J. Phys.: Conf. Ser*. **300**, 012017 (2011)
[23] M Jones and J Tennyson, *J. Phys. B: At. Mol. Opt. Phys*. **43**, 045101 (2010)
[24] D Gorfinkiel and J Tennyson, *J. Phys. B: At. Mol. Opt. Phys*. **37**, L343 (2004)
[25] D Gorfinkiel and J Tennyson, *J. Phys. B: At. Mol. Opt. Phys*. **38**, 1607 (2005)
[26] K N Joshipura and N Mason, *Atomic-molecular ionisation by electron scattering: Theory and applications* (Cambridge University Press, 2018)
[27] F Blanco and G Garcia, *Phys. Lett. A* **317**, 458 (2003)
[28] F Blanco and G Garcia, *J. Phys. B* **42**, 145203 (2009)
[29] F Blanco, J Rosado, A Illana and G Garcia, *Phys. Lett. A* **374**, 4420 (2010)
[30] A Jain and K L Baluja, *Phys. Rev. A* **45**, 202 (1992)
[31] W Y Baek, A Arndt, M U Bug, H Rabus and M Wang, *Phys. Rev. A* **88**, 032702 (2013)
[32] M Kaur, G Kaur, A K Jain, H Mohan, P S Singh, S Sharma and K L Baluja, *Phys. Rev. A* **97**, 052711 (2018)
[33] G Kaur, A K Jain, H Mohan, P S Singh, S Sharma and A N Tripathi, *Phys. Rev. A* **91**, 022702 (2015)
[34] F A Gianturco, V Di Martino and A Jain, *Il Nuovo Cimento D* **14(4)**, 411 (1992)
[35] W M Huo and F A Gianturco (Eds) *Computational methods for electron molecule collisions* (Plenum, New York, 1994)
[36] F A Gianturco and A Jain, *Phys. Rep.* **143**, 347 (1986)
[37] F A Gianturco, R R Lucchese, N Sanna and A Talamo, A generalized single centre approach for treating electron scattering from polyatomic molecules, in: *Electron collisions with molecules, clusters and surfaces*, edited by H Ehrhardt and L A Morgan (Plenum, New York, 1994)
[38] Y-K Kim and M E Rudd, *Phys. Rev. A* **50**, 3954 (1994)
[39] J M Carr, P G Galiatsatos, J D Gorfinkiel, A G Harvey, M A Lysaght, D Madden, Z Masn, M Plummer and J Tennyson, *Eur. Phys. J. D* **66**, 58 (2012)
[40] Z Masin, J Benda, J D Gorfinkiel, A G Harvey and J Tennyson, *Comput. Phys. Commun*. **249**, 107092 (2020)
[41] https://ccpforge.cse.rl.ac.uk/gf/project/ukrmol-in
[42] N Sanna and F A Gianturco, *Comput. Phys. Commun*. **128**, 139 (2000)
[43] M Tinkham, *Group theory and quantum mechanics* (McGraw-Hill, New York, 1964)
[44] J P Perdew and A Zunger, *Phys. Rev. B* **23**, 5048 (1981)
[45] S Hara, *J. Phys. Soc. Jpn.* **22**, 710 (1967)
[46] N Sanna and F A Gianturco, *Comput. Phys. Commun*. **114**, 142 (1998)
[47] A Bharadvaja, S Kaur and K L Baluja, *Phys. Rev. A* **91**, 032701 (2015)
[48] A Bharadvaja, S Kaur and K L Baluja, *Pramana – J. Phys*. **89(2)**: 30 (2017)
[49] I Fabrikant, *J Phys. B: At. Mol. Opt. Phys*. **49**, 222005 (2016)
[50] L Alvarez, F Costa, A I Lozano, J C Oller, A Munoz, F Blanco, P Limao-Vieira, R D White, M J Brunger and G Garcia, *Phys. Chem. Chem. Phys*. **22**, 13505 (2020)
[51] S Stefanowska-Tur, P Mozejko, E Ptasinska-Denga and C Szmytkowski, *J. Chem. Phys*. **150**, 094303 (2019)
[52] GAUSSIAN 03, Gaussian, Inc, Wallingford, CT
[53] N Sanna, I Baccarelli and G Morelli, *Comput. Phys. Commun*. **180**, 2544 (2009)
[54] M H Rees, *Physics and chemistry of the upper atmosphere* (Cambridge University Press, Cambridge, 1999)
[55] J L de Pablos, P A Kendall, P Tegeder, A Williart, F Blanco, G Garcia and N J Mason, *J. Phys. B* **35**, 865 (2002)
[56] K N Joshipura, B K Antony and M Vinodkumar, J. *Phys. B* **35**, 4211 (2002)
[57] T W Shyn and C J Sweeney, *Phys. Rev. A* **47(4)**, 2919 (1993)
[58] S Kumar, *Nature (London)* **280**, 758 (1979)
[59] F Darrell, F Strobel and J Davis, *Astrophys. J*. **238**, L49 (1980)
[60] A F Cheng, *Astrophys. J*. **242**, 812 (1980)
[61] J Marling, *IEEE J. Quantum Electron.* **14**, 4 (1978)
[62] D Klee and H Hocker, *Adv. Polym. Sci*. **149**, 1 (1999)
[63] I Gallinberti, *Pure Appl. Chem*. **60**, 663 (1988)
[64] S Trajmar and T W Shyn, *J. Phys. B* **22**, 2911 (1989)
[65] R J Gulley and S J Buckman, *J. Phys. B* **27**, 1833 (1994)
[66] F A Gianturco, P Paioletti and N Sanna, *J. Phys. B: At. Mol. Opt. Phys*. **30**, 4535 (1997)
[67] K N Joshipura and S Gangopadhyay, *J. Phys. B* **41**, 215205 (2008)

[68] M Vinodkumar, C Limbachiya, A Barot and N Mason, *Phys. Rev. A* **86**, 012706 (2012)
[69] M Hayashi, Electron collision cross-sections for molecules determined from beam and swarm data, in: *Swarm studies and inelastic electron-molecule collisions* edited by L C Pitchford, B V McKoy, A Chutjian and S Trajmar (Springer-Verlag, New York, 1987)
[70] T Meltzer, J Tennyson, Z Masin, M C Zammit, L H Scarlett, D V Fursa and I Bray, *J. Phys. B: At. Mol. Opt. Phys*. **53**, 145204 (2020)
[71] R Zhang, A Faure and J Tennyson, *Phys. Scr*. **80**, 015301 (2009)
[72] Y K Kim, W Hwang, N M Weinberger, M A Ali and M E Rudd, *J. Chem. Phys.* **106**, 1026 (1997)
[73] https://physics.nist.gov/PhysRefData/ionisation/molTable.html
[74] A Zecca, J C Nogueira, G P Karwasz and R S Brusa, *J. Phys. B* **28**, 477 (1995)
[75] C Szmytkowski, P Mozejko and A Krzysztofowicz, *Radiat. Phys. Chem*. **68**, 307 (2003)
[76] Z Masin, J Benda, A G Harvey, A Al-Refaie, J D Gorfinkiel and J Tennyson, UKRMol+: UKRMol-in (Version 3.0). Zenodo. https://doi.org/10.5281/zenodo.3371125